Product Formation in the Cl-Initiated Oxidation of Cyclopropane

John D. DeSain,† Stephen J. Klippenstein, and Craig A. Taatjes*

Combustion Research Facility, Mail Stop 9055, Sandia National Laboratories, Livermore, California 94551-0969

Michael D. Hurley and Timothy J. Wallington

Research Staff, Ford Motor Company, SRL-3083, Dearborn, Michigan 48121-2053

Received: September 23, 2002; In Final Form: December 31, 2002

The production of HO_2 and OH in the reaction of c-$C_3H_5 + O_2$ is investigated as a function of temperature (296−700 K) using laser photolysis/CW infrared frequency modulation spectroscopy. The cyclopropyl radical is generated by the Cl + cyclopropane reaction following pulsed laser photolysis of Cl_2. Significant OH and HO_2 production is observed at 296 K, and both $[OH]/[Cl]_0$ and $[HO_2]/[Cl]_0$ increase slowly with increased temperature until ∼600 K, where a sharper increase with temperature is observed. Relative rate and end product measurements are also performed using a smog chamber FTIR apparatus. The relative reactivity of cyclopropyl radicals toward O_2 and Cl_2 is $k_{c\text{-}C_3H_5+O_2}/k_{c\text{-}C_3H_5+Cl_2} = 0.44 \pm 0.02$ at 700 Torr, 0.44 ± 0.03 at 75 Torr, and 0.24 ± 0.02 at 10 Torr of N_2 diluent at 296 K. Ethene and oxirane are identified as end products of the cyclopropane oxidation. Molar yields of oxirane are 0.11 ± 0.03 at 6 Torr, 0.08 ± 0.02 at 10 Torr, and 0.06 ± 0.02 at 50 Torr total pressure of N_2/O_2 diluent; molar yields of ethene are 0.14 ± 0.02 (6 Torr) and 0.15 ± 0.01 (10 Torr) and 0.30 ± 0.06 (50 Torr). The combined experimental data suggest that HO_2 is not a primary product of the cyclopropyl + O_2 reaction but arises from secondary reactions of HCO or HCO_2 products formed in conjunction with oxirane or ethene. Quantum chemical calculations of stationary points on the cyclopropyl + O_2 surface indicate that ring opening and isomerization of c-$C_3H_5O_2$ to form a dioxirane species is possible, with a calculated transition state energy 0.5 kcal mol^{-1} above that of the reactants. This dioxirane species is a conceivable precursor to HCO_2 + ethene or HCO + oxirane formation; however, the calculations suggest OH + acrolein as the dominant bimolecular products.

1. Introduction

Alkyl radical (R) reactions with molecular oxygen are central to understanding hydrocarbon oxidation in combustion systems and in the atmosphere. The most detailed studies of $R + O_2$ reactions have focused on understanding the mechanism of the smaller straight-chain alkyl (ethyl and propyl) reactions with O_2.[1−8] The $R + O_2$ reactions proceed via a bound alkylperoxy (RO_2) radical, which can subsequently eliminate HO_2 to form a conjugate alkene or isomerize by intramolecular hydrogen abstraction to form a hydroperoxyalkyl radical (often denoted QOOH). The QOOH radical can in turn react with O_2 or dissociate to form HO_2 + alkene or OH + cyclic ether products. The branching among these channels is important for chain propagation in low-temperature hydrocarbon oxidation because of the differing reactivities of OH and HO_2. Reactions of QOOH are thought to lead to chain branching in low-temperature oxidation, making understanding the formation of QOOH important for modeling autoignition and engine knock.

The alkene + HO_2 channel largely dominates the reactions of small alkyl radicals with O_2 for moderate temperatures.[1−3,5−21]

$$\text{alkyl} + O_2 \rightarrow \text{alkene} + HO_2 \qquad (1)$$

For example, Walker and Morley[22] report high alkene yields at 753 K and 70 Torr from $C_2H_5 + O_2$ (99%), t-$C_4H_9 + O_2$ (99%), and c-$C_5H_9 + O_2$ (90%). The principal other products are cyclic ethers arising from isomerization to QOOH. The elimination of HO_2 and the various isomerizations to form QOOH species occur through ring transition states, and the facility of these reactions may be affected by cyclization of the alkyl species. Several recent studies have investigated the oxidation of cyclic alkanes such as cyclopentane[12,15,23] and cyclohexane.[24] Time-resolved probing of HO_2 product formation in Cl-initiated cyclopentane oxidation suggests that, while the energetics of the HO_2 elimination are similar to that in ethyl and propyl + O_2, the pre-exponential factor is larger for the cyclic alkyl radical.[12] Because in cyclic alkyl RO_2 species rotation around C−C bonds is already hindered, the entropy loss between reactant and the ring transition state for elimination is smaller than that for acyclic RO_2 species, which lose an internal rotation in reaching the transition state.

Little is known about the oxidation of the smallest ring alkane, cyclopropane, although Falconer, Knox, and Trotman-Dickenson[25] measured the total cyclopropane oxidation rate relative to that for ethane oxidation between 601 and 689 K. If the reaction of the cyclopropyl radical with O_2 is similar to other $R + O_2$ reactions, then the major product channels would be

$$c\text{-}C_3H_5 + O_2 \overset{M}{\leftrightarrow} c\text{-}C_3H_5O_2 \qquad (2a)$$

$$\rightarrow c\text{-}C_3H_4 + HO_2 \qquad (2b)$$

$$\rightarrow c\text{-}C_3H_4O + OH \qquad (2c)$$

* To whom correspondence should be addressed. Electronic mail: cataatj@sandia.gov.

† Present address: The Aerospace Corporation, 2350 E. El Segundo Blvd., El Segundo, CA 90245-4691.

10.1021/jp022120u CCC: $25.00
Published on Web 03/04/2003

TABLE 1: Estimated ΔH_r°(298) for Several Possible c-C_3H_5 + O_2 Reaction Pathways[a]

reaction products	ΔH_r° (kcal mol^{-1})
allyl (CH_2CHCH_2) + O_2	−29.0
cyclopropene (c-C_3H_4) + HO_2	0.5
propyne ($CHCCH_3$) + HO_2	−22.8
allene (CH_2CCH_2) + HO_2	−21.8
acrolein (CH_2CHCHO + OH)	−76.6
cyclopropanone (c-C_3H_4O) + OH	−49.1
acetaldehyde (CH_3CHO) + HCO	−100.4
oxirane (C_2H_4O) + HCO	−73.6
ethene (C_2H_4) + HOCO	−104.9
cyclopropoxy (c-C_3H_5O) + O	6.2
formaldehyde (H_2CO) + H_2CCHO	−93.0

[a] Thermochemistry data from HL2 calculations.

However, production of cyclopropene + HO_2 from cyclopropyl + O_2 is predicted to be slightly endothermic. Also, the cyclopropyl radical contains a large amount of potential energy in the form of ring strain, and ring-opening may make other products possible. Without a low-energy path to HO_2 + alkene products, cyclopropyl + O_2 may follow a significantly different reaction mechanism than other alkyl + O_2 reactions.

The present work uses a combination of experimental and theoretical methods to investigate the mechanism of the cyclopropyl + O_2 reaction. The time behavior of HO_2 and OH formation in the Cl-initiated oxidation of c-C_3H_6 is measured between 296 and 700 K by using infrared spectroscopy following pulsed photolytic initiation. The reaction is observed to produce a significant amount of both OH and HO_2 even at 296 K. The formation of HO_2 has some qualitative similarities to that observed in previous experiments on C_2H_5 + O_2,[2] C_3H_7 + O_2,[1] c-C_5H_9 + O_2,[12] and C_4H_9 + O_2.[13] However, the observation of significant OH formation at such a low temperature is peculiar to cyclopropyl + O_2. Smog chamber/FTIR measurements show that ethene and oxirane are products of cyclopropane oxidation at 296 K. Ab initio characterization of stationary points on the cyclopropyl−O_2 potential energy surface provides an explanation for the observed products. It is proposed that HO_2 is not a primary product of the cyclopropyl + O_2 reaction but results from secondary reactions of HCO or HCO_2 products formed in coincidence with oxirane or ethene.

2. Experimental Section

2.1. Laser Absorption Measurements at Sandia National Laboratories. The reaction of c-C_3H_5 + O_2 is investigated by Cl-initiated oxidation of cyclopropane, using a laser photolysis/CW infrared frequency modulation method similar to that employed previously.[1,2,12,13] The Cl is generated by 355 nm photolysis of Cl_2, and c-C_3H_5 is formed by the reaction of Cl with cyclopropane. The c-C_3H_5 radical then reacts with O_2:

$$Cl_2 \xrightarrow{h\nu\ (355\ nm)} 2Cl \qquad (3)$$

$$Cl + c\text{-}C_3H_6 \rightarrow c\text{-}C_3H_5 + HCl \qquad (4)$$

$$c\text{-}C_3H_5 + O_2 \rightarrow \text{products} \qquad (2)$$

Experimental heats of formation are unavailable for many possible products of reaction 2; estimated thermochemistries for several conceivable channels are listed in Table 1.

To minimize the effects of the competing reaction of Cl_2 with c-C_3H_5, the O_2 concentration is kept at least 30 times greater than the Cl_2 concentration. The rate constant for c-C_3H_5 + Cl_2 is larger than that of c-C_3H_5 + O_2 at 298 K (see below), but the Cl product of the c-C_3H_5 + Cl_2 reaction regenerates c-C_3H_5 radicals, and the chain chlorination is soon quenched by the oxidation. Because of the relatively low rate coefficient for the reaction of cyclopropane with Cl (k_4(298 K) = (1.15 ± 0.17) × 10^{-13} cm^3 molecule^{-1} s^{-1};[26] $k = (8.96 \times 10^{-11})e^{(-2080K/T)}$ cm^3 molecule^{-1} s^{-1}),[27] a large excess of cyclopropane ((0.8−5) × 10^{16} cm^{-3}) is used. Nevertheless, at room temperature the contribution of the reaction of Cl with HO_2 is not completely negligible. This reaction may reduce the apparent HO_2 yield from the c-C_3H_5 + O_2 reaction slightly, although no significant difference in apparent yield is noted over the range of [c-C_3H_6] employed in the present experiments.

The formation of HO_2 is monitored by infrared absorption of the overtone of the O−H stretch in HO_2 near 1.5 μm using a tunable diode laser, and the formation of OH is monitored by direct absorption on the P(2.5)1$^-$ line of the vibrational fundamental at 3484.6 cm^{-1} using an F-center laser. Two-tone frequency modulation of the diode laser probe is employed to increase the signal-to-noise ratio of the HO_2 measurement. For the OH measurement a balanced detector method is employed, where the first detector (reference) monitors a portion of the laser output prior to entering the cell and the second (signal) monitors the infrared beam after passing through the reactor. The average DC power on the two detectors is equalized and the signals from the two detectors are subtracted to reduce the contribution of laser amplitude noise.

The experiments are performed in a resistively heated quartz slow-flow reactor. The IR probes are placed on the same path through the reactor by using polarizing prisms to combine and separate the beams. The IR probes are passed multiple times through the reactor by using a Herriott-type multipass cell, in which the probe beams intercept the UV photolysis beam only in the center of the flow cell, where the temperature is more readily controlled. Typical gas concentrations are as follows: O_2, 6.4 × 10^{16} cm^{-3}; Cl_2, 2.0 × 10^{15} cm^{-3}; cyclopropane, 8 × 10^{15} to 5 × 10^{16} cm^{-3}. Helium is added to reach a total density of 8.5 × 10^{17} cm^{-3}. Gases are obtained from commercial sources at the following stated purities: O_2, >99.998%; Cl_2, >99.99%; He, >99.9999%; cyclopropane, >99.9%. Major impurities in the cyclopropane sample, as characterized by GC/MS, are 1,1- and 1,3-dichloropropane, with smaller amounts of propene and n-propanol. The contribution of Cl reaction with n-propanol impurity is of most concern for the HO_2 production measurements, since its rate constant is ∼1250 times that of Cl + cyclopropane[28,29] and because the product hydroxypropyl radical could, by analogy with CH_2OH, rapidly produce HO_2 by reaction with oxygen.[30] Reactions of Cl with the other impurities will produce substituted propyl radicals, which are not expected to produce significant HO_2 at low temperature.[1,4] The relative importance of Cl reactions with impurities will be greater at lower temperature, since the Cl + cyclopropane reaction has a significant activation energy. Comparison of the apparent room temperature rate coefficient measured by following HCl appearance with that determined by relative rate methods directly monitoring cyclopropane disappearance, detailed in the accompanying paper, suggests an upper limit for the contributions of reactions with impurities of ∼20%. The consequences of these reactions are relatively minor and are described in the Discussion section below.

The HO_2 signal produced by the c-C_3H_5 + O_2 reaction is scaled to the initial Cl concentration by comparison with the HO_2 signal from the $Cl_2/CH_3OH/O_2$ system under identical photolysis conditions. This reaction system is assumed to convert

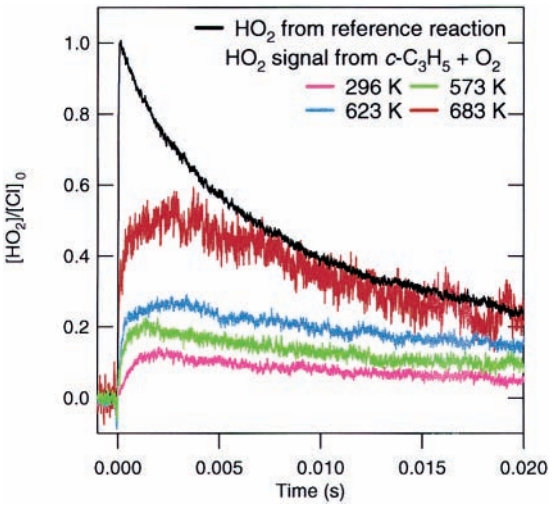

Figure 1. Scaled HO_2 signals at 296 K (magenta), 573 K (green), 623 K (cyan), and 683 K (red) from the reaction of c-$C_3H_5 + O_2$ with [c-C_3H_6] of 8×10^{15} cm^{-3} and a total density of 8.5×10^{17} cm^{-3}. The scaled HO_2 signal from the reaction of $CH_2OH + O_2$ at 296 K and a total density of 8.5×10^{17} cm^{-3} is shown in black. The signals are scaled to the initial Cl atom concentration as described in the text.

100% of the initial Cl atoms ($\equiv$ [Cl]$_0$) to HO_2 over the temperature range of concern:[30]

$$Cl_2 \xrightarrow{h\nu\ (355\ nm)} 2Cl \qquad (3)$$

$$CH_3OH + Cl \rightarrow CH_2OH + HCl \qquad 100\% \qquad (5)$$

$$CH_2OH + O_2 \rightarrow CH_2O + HO_2 \qquad 100\% \qquad (6)$$

Using $k(CH_2OH + Cl_2)/k(CH_2OH + O_2) = 2.8$[31] and $[O_2]/[Cl_2] = 30$, it follows that approximately 90% of CH_2OH radicals react with O_2 while 10% react with Cl_2. However, the $CH_2OH + Cl_2$ reaction regenerates Cl atoms which react with methanol to regenerate CH_2OH radicals. Therefore, the $CH_2OH + Cl_2$ reaction slightly decreases (by $\sim$ 10%) the effective rate of the $CH_2OH + O_2$ reaction, which is of no consequence to the present analysis. Dividing the HO_2 signal from c-$C_3H_5 + O_2$, $I(t)$, by the peak amplitude of the reference HO_2 signal, A_{HO_2}, expresses the amplitude of the HO_2 signal from c-$C_3H_5 + O_2$ in terms of [HO_2]/[Cl]$_0$:

$$\frac{I(t)}{A_{HO_2}} = \frac{\alpha[HO_2]_t}{\alpha[Cl]_0} = \frac{[HO_2]_t}{[Cl]_0} \qquad (7)$$

where α is a proportionality constant relating the observed FM signal to the concentration of HO_2. Representative time-resolved FM signals are shown in Figure 1.

If the amplitude of the scaled HO_2 signal from c-$C_3H_5 + O_2$ is to be related to a yield of HO_2 in reaction 2, corrections must be made for consumption reactions of HO_2 that occur on the time scale of the HO_2 formation. Correction for the HO_2 self-reaction is straightforwardly accomplished by using the effective rate constant provided by the reference signal, whose decay is dominated by the $HO_2 + HO_2$ reaction, as shown in previous $R + O_2$ investigations.[1,2,12,13] However, the HO_2 formed in the c-$C_3H_5 + O_2$ reaction suffers additional HO_2 removal reactions not present in the reference system, such as $HO_2 + OH$ and $HO_2 + c$-$C_3H_5O_2$. Therefore, the peak amplitude of the scaled HO_2 signal is a lower limit to the total amount of HO_2 formed during the experiment. The production of significant OH in the Cl_2/c-C_3H_6/O_2 system also complicates the interpretation of the HO_2 amplitude. In previous investigations of $R + O_2$ reactions, it has been possible to simply model the RO_2 and HO_2 reactions to extract an overall HO_2 yield.[1,2,12] In the cyclopropane system the production of significant OH requires a more complex system of reactions and (unknown) rate coefficients. Because of these complications, in the present system we simply list the peak [HO_2]/[Cl]$_0$ (corrected only for the self-reaction) in Table 2, which is a lower limit on the overall HO_2 yield. It should be emphasized that the HO_2 yield in the present case is a measure of the fraction of the initial Cl concentration that is converted to HO_2 in the course of the overall oxidation, and cannot be simply interpreted as the branching fraction of an elementary reaction.

TABLE 2: Peak Amplitude of the Scaled HO_2 Signal from c-$C_3H_5 + O_2$

temp (K)	peak [HO_2]/[Cl]$_0$
296	0.12 ± 0.03
373	0.17± 0.04
473	0.20 ± 0.04
573	0.19 ± 0.04
623	0.26 ± 0.05
638	0.36 ± 0.07
653	0.42 ± 0.08
663	0.38 ± 0.08
668	0.48 ± 0.08
683	0.55 ± 0.09
698	0.44 ± 0.09

The observed OH signal from c-$C_3H_5 + O_2$ can be scaled by using the same reference reaction, by reacting the HO_2 formed from the reference reaction with NO to form OH radicals.[30]

$$HO_2 + NO \xrightarrow{100\%} OH + NO_2 \qquad (8)$$

CH_3OH is in significant excess over NO, so there is no complication from the relatively slow Cl + NO reaction.[30] The peak of the OH signal from the reference reaction cannot be used directly to scale the OH signal from c-$C_3H_5 + O_2$. The OH signal obtained from the reference system must be modeled to account for removal reactions, which reduce the peak amplitude of the signal. The OH signal from the reference system is modeled using the reactions listed in Table 3. Figure 2 shows observed and modeled OH signals from the reference reaction system at 296, 373, and 573 K. The radical density was calculated from the second-order decay of the HO_2 signal observed without added NO, using the literature rate constant value for $HO_2 + HO_2$ (listed in Table 3). Typical radical densities in the OH/HO_2 IR experiments are between 3×10^{13} and 8×10^{13} cm^{-3}. As seen in Figure 2, the model accurately predicts the observed formation rate of the OH signal but overestimates the rate of decay. A better fit can be obtained by adjusting the rate coefficient for the NO + OH + M reaction, which is the major loss mechanism of OH at long times. However, since modeling the peak height and hence the [OH]/[Cl]$_0$ ratio is the major concern, the literature reaction rate constants are used without alteration. The fitted OH signals in Figure 2 correspond to a peak OH concentration of from 0.32 to 0.50 $\times$ [Cl]$_0$ in the reference reaction system, depending on the temperature and concentrations used in each individual trial. The ratio of the peak [OH] concentration to the initial [Cl]$_0$ predicted by the model ([OH]$_{pk}$/[Cl]$_0$)$_{model}$ is then used to scale the OH signal ($I_{OH}(t) \equiv \alpha'$[OH]$_t$) observed from the Cl_2/c-C_3H_6/O_2 system under identical photolysis conditions (and hence

TABLE 3: Reactions and Rate Constants Used To Model the OH Signal Generated from the $Cl_2/CH_3OH/O_2/NO$ System[a]

reaction	A^b	n	E_a/R (K)	k (298 K)^b	ref
$CH_3OH + Cl \rightarrow HCl + CH_2OH$	5.4×10^{-11}			5.4×10^{-11}	30
$CH_2OH + O_2 \rightarrow HO_2 + CH_2O$	3.77×10^{-15}	5.94	2284	8.13×10^{-12}	54
$HO_2 + NO \rightarrow OH + NO_2$	3.5×10^{-12}		250	8.10×10^{-12}	30
$HO_2 + HO_2 \rightarrow O_2 + H_2O_2$[c]	2.2×10^{-13}		599	1.66×10^{-12}	28
$OH + HO_2 \rightarrow H_2O + O_2$	4.8×10^{-11}		250	1.11×10^{-10}	28
$OH + CH_3OH \rightarrow CH_2OH + H_2O$	2.12×10^{-13}	2.65	444	9.40×10^{-13}	55
$OH + NO + M \rightarrow HNO_2 + M$	2.79×10^{-32}		−806	4.3×10^{-31}	56
$OH + OH \rightarrow O + H_2O$	7.89×10^{-14}	2.60	945	1.88×10^{-12}	28
$OH + OH + M \rightarrow M + H_2O_2$	6.89×10^{-31}	−0.80		6.89×10^{-31}	28
$OH + CH_2O \rightarrow HCO + H_2O$	4.73×10^{-12}	1.18	225	1.01×10^{-11}	57
$OH + HCO \rightarrow CO + H_2O$	1.70×10^{-10}			1.70×10^{-10}	57
$OH + NO_2 + M \rightarrow HNO_3 + M$	2.60×10^{-30}	−2.90		2.60×10^{-30}	28
$OH + HNO_2 \rightarrow H_2O + NO_2$	6.24×10^{-12}	1	68	4.97×10^{-12}	58
$HCO + O_2 \rightarrow HO_2 + CO$	5.60×10^{-12}			5.60×10^{-12}	59
$NO + CH_2OH \rightarrow CH_2OH(NO)$	2.50×10^{-11}			2.50×10^{-11}	60

[a] The rate constants are written in the form $A(T/296)^n e^{(-E_a/RT)}$. [b] Units are (cm^3 $molecule^{-1}$ s^{-1}) for second-order reactions and (cm^6 $molecule^{-2}$ s^{-1}) for third-order reactions. [c] The rate constant has a pressure dependent term; $k = (4.5 \times 10^{-32})[M] + (2.2 \times 10^{-13})e^{(599K/T)}$.

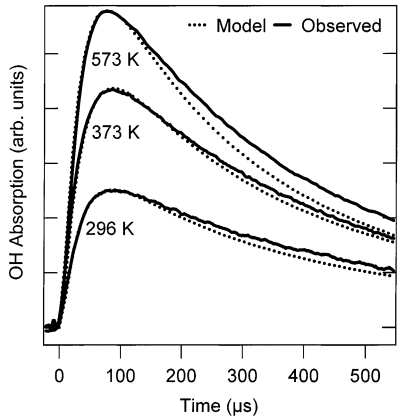

Figure 2. Time-resolved infrared OH signals from $CH_2OH/NO/O_2$ taken at 296, 373, and 573 K at a total density of 8.5×10^{17} cm^{-3}. The dashed lines represent the OH signals predicted by the model described in the text. The peaks of the modeled curves represent the peak $[OH]/[Cl]_0 = 0.45$ (296 K), 0.40 (373 K), and 0.35 (573 K).

identical initial Cl concentrations):

$$\frac{[OH]_t}{[Cl]_0} \cong \frac{I_{OH}(t)}{A_{OH}}\left(\frac{[OH]_{pk}}{[Cl]_0}\right)_{ref,model} \quad (9)$$

Here A_{OH} ($\equiv \alpha'[OH]_{pk,ref}$) is the observed peak amplitude of the OH signal from the reference reaction, and α' is the constant of proportionality between OH concentration and the observed absorption signal, which includes absorption strength, line shape, and instrument functions. Table 4 lists the peak amplitude of the scaled OH signal from c-$C_3H_5 + O_2$ for several temperatures.

The peak of the scaled OH signal should be significantly smaller than the OH branching fraction, as the OH radicals are removed at a significant rate compared to that of their formation. Figure 3 compares the absorption signal for OH in Cl-initiated oxidation of cyclopropane with the infrared FM signal for HO_2 under the same conditions. The peak amplitude of the OH signal occurs at an earlier time than the peak amplitude of the HO_2 signal because of the more rapid removal of OH. The ratio of peak concentration to actual branching fraction will also be smaller for OH than for HO_2.

2.2. FTIR Smog Chamber System at Ford Motor Company. Experiments are performed in a 140-L Pyrex reactor interfaced to a Mattson Sirus 100 FTIR spectrometer described elsewhere.[32] The reactor is surrounded by 22 fluorescent black lamps (GE F15T8-BL), which are used to photochemically initiate the experiments. Cl atoms were generated by photolysis of molecular chlorine in 700 Torr total pressure of N_2 diluent at 295 ± 2 K.

$$Cl_2 + h\nu \rightarrow 2Cl \quad (3)$$

Loss of c-C_3H_6 and formation of products were monitored by

TABLE 4: Individual Determinations of the Peak Amplitude of the Scaled OH Signal from c-$C_3H_5 + O_2$

temp (K)	peak ratio[a]	modeled $[OH]_{pk,ref}/[Cl]_0$	peak $[OH]/[Cl]_0$
296	0.09	0.45	0.04
296	0.04	0.45	0.02
296	0.08	0.45	0.04
373	0.10	0.40	0.04
373	0.05	0.47	0.03
473	0.13	0.43	0.05
473	0.11	0.40	0.04
473	0.14	0.35	0.05
573	0.15	0.32	0.05
573	0.13	0.41	0.05
598	0.18	0.39	0.07
623	0.17	0.39	0.07
648	0.19	0.39	0.07
663	0.23	0.38	0.09
678	0.23	0.40	0.09
698	0.28	0.40	0.11

[a] Ratio of the peak OH signal from Cl_2/c-C_3H_6/O_2 to the peak OH signal from the reference $Cl_2/CH_3OH/O_2/NO$ system.

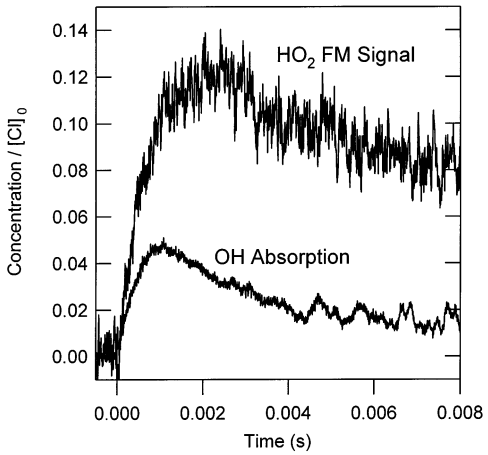

Figure 3. OH absorption signal compared to the HO_2 FM signal from the reaction of c-$C_3H_5 + O_2$ at 296 K and a total density of 8.5×10^{17} cm^{-3}. The signals are scaled to the initial Cl atom concentration as described in the text.

Fourier transform infrared spectroscopy using an infrared path length of 27.5 m and a spectral resolution of 0.25 cm^{-1}. Infrared spectra were derived from 32 coadded interferograms. Reagents were obtained from commercial sources at the following stated purities (cyclopropane (>99.9%); chlorine (>99.99%); N_2 (UHP); O_2 (UHP)) and were used as received.

In smog chamber experiments, unwanted loss of reactants and products by photolysis, dark chemistry, and wall reaction have to be considered. Control experiments were performed to check for these losses. Mixtures of *c*-C_3H_6 and air were subjected to UV irradiation for 5 min and then left in the dark for 30 min. There was no observable loss (<2%) of *c*-C_3H_6. There was no observable loss (<2%) of *c*-C_3H_5Cl when mixtures containing this compound were left in the chamber in the dark for 45 min. Heterogeneous reactions are not a significant complication in the present work.

2.3. Ab Initio Calculations. The geometric structures and vibrational frequencies for all stationary points considered here are obtained via density functional theory employing the Becke-3 Lee-Yang Parr (B3LYP) functional.[33] The calculations denoted HL1, described below, employ the 6-31G* basis set for the structures and frequencies, while those designated HL2 employ the 6-311++G(d,p) basis.[34] The connections of each saddle point to its local minima are generally estimated via visualization of the corresponding imaginary vibrational mode. For a few uncertain cases intrinsic reaction coordinate calculations are also performed.

Higher-level energies are obtained via two separate methods. Both methods employ a combination of quadratic configuration interaction calculations with perturbative inclusion of the triplet contribution, QCISD(T),[35] and second-order Møller Plesset perturbation theory (MP2).[34] In the first method, referred to as HL1, the 6-311G(d,p) basis set is employed for the QCISD(T) calculations, and the 6-311++G(3d*f*,2pd) basis set is employed for the MP2 calculations. Also, the core electrons are treated as active in the MP2 evaluations for the latter basis set. Approximate QCISD(T,Full)/6-311++G(3df,2pd) estimates, E_{HL1}, are then obtained as

$$E_{HL1} = E[\text{QCISD(T)/6-311G(d,p)}] + E[\text{MP2(Full)/6-311++G(3df,2pd)}] - E[\text{MP2/6-311G(d,p)}] \quad (10)$$

For the most important transition states, and for the bimolecular reaction exothermicities, we also implement a second method, which should have somewhat reduced uncertainties. In this method the infinite basis set limit is estimated via the extrapolation of results obtained for sequences of the correlation consistent polarized valence basis sets. The extrapolation is obtained from the expression[36]

$$E(\infty) = E(l_{max}) - B/(l_{max} + 1)^4 \quad (11)$$

where l_{max} is the maximum angular momentum in the basis set. The QCISD(T) extrapolation is obtained on the basis of calculations with Dunning's[37] correlation consistent polarized valence double-ζ (cc-pvdz) and triplet-ζ (cc-pvtz) basis sets, with $l_{max} = 2$ and 3, respectively. An MP2 calculation with the correlation consistent polarized valence quadruple-ζ basis (cc-pvqz) ($l_{max} = 4$) allows for two separate MP2 extrapolations; one from the cc-pvdz, cc-pvtz pair and one from the cc-pvtz, cc-pvqz pair. The final higher level estimate, E_{HL2}, is obtained as the sum of the QCISD(T) extrapolation and the difference between the two MP2 extrapolations. This combination of extrapolations can be expressed as

$$E_{HL2} = E[\text{QCISD(T)/cc-pvtz}] + \{E[\text{QCISD(T)/cc-pvtz}] - E[\text{QCISD(T)/cc-pvdz}]\} \times 0.46286 + E[\text{MP2/cc-pvqz}] + \{E[\text{MP2/cc-pvqz}] - E[\text{MP2/cc-pvtz}]\} \times 0.69377 - E[\text{MP2/cc-pvtz}] - \{E[\text{MP2/cc-pvtz}] - E[\text{MP2/cc-pvdz}]\} \times 0.46286 \quad (12)$$

Zero-point energy changes are evaluated at the B3LYP level and are incorporated in the final energies reported below. The Gaussian-98 quantum chemistry software was employed in all the quantum chemistry calculations described here.[38]

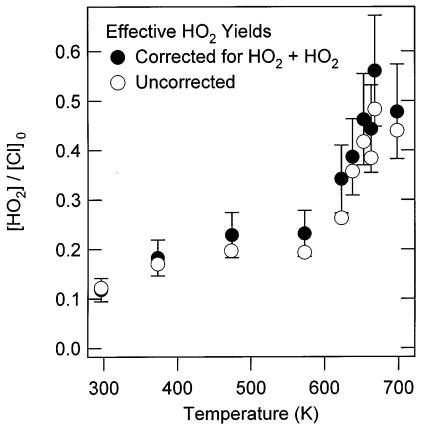

Figure 4. Peak amplitude of the scaled HO_2 signal from *c*-$C_3H_5 + O_2$ at a total density of 8.5×10^{17} cm^{-3} as a function of temperature. The amplitudes are corrected for the HO_2 self-reaction and scaled to the initial Cl atom concentration as described in the text.

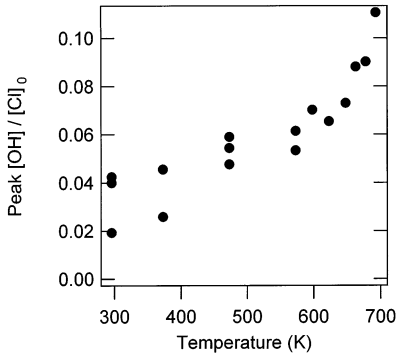

Figure 5. Peak amplitude of the scaled OH signal from *c*-$C_3H_5 + O_2$ as a function of temperature. The signals are scaled to the initial Cl atom concentration as described in the text.

3. Results

3.1. Measurement of HO_2 and OH Formation at Sandia. Figure 4 shows the temperature dependence of the peak amplitude of the HO_2 signal from *c*-$C_3H_5 + O_2$. The HO_2 peak amplitudes increase slightly from 0.12 to 0.20 between 296 and 600 K. Between 600 and 700 K the HO_2 peak amplitude begins to increase more sharply from 0.20 at 600 K to ~0.50 at 700 K. As seen in Figure 5 the temperature dependence of the OH peak amplitudes is similar to that of the HO_2 peak heights. The OH peak amplitudes increase moderately in the 296 K to 600 K range. Between 600 and 700 K the OH peak amplitudes increase more sharply with increasing temperature.

In previous investigations of R + O_2 reactions, the HO_2 signal in the 296 K to 550 K temperature range was formed nearly

instantaneously after the UV photolysis pulse. Because the hydrogen abstraction reaction Cl + *c*-C_3H_6 is much slower than the hydrogen abstraction by Cl from other alkanes (1.15×10^{-13} cm^3 $molecule^{-1}$ s^{-1} for *c*-C_3H_6 + Cl compared to 5.7×10^{-11} cm^3 $molecule^{-1}$ s^{-1} for C_2H_6 + Cl at 296 K),[26,30,39] the initial rise time of the HO_2 signal at 296 K is resolved in the present experiments (see Figure 1). The HO_2 and OH formation rates at 296 K increase as the concentration of the cyclopropane is increased. The rise time of the OH and HO_2 signals at 296 K is consistent with the measured Cl + *c*-C_3H_6 rate constants of Baghal-Vayjooee and Benson at 296 K ($(1.21 \pm 0.05) \times 10^{-13}$ cm^3 $molecule^{-1}$ s^{-1})[40] and the measurements reported in the accompanying paper ($(1.15 \pm 0.17) \times 10^{-13}$ cm^3 $molecule^{-1}$ s^{-1}).[26] Using the measured pseudo-first-order rate constants for HO_2 formation, a second-order rate constant for the reaction *c*-C_3H_6 + Cl of $k_4 = (1.36 \pm 0.40) \times 10^{-13}$ cm^3 $molecule^{-1}$ s^{-1} is obtained. This suggests that cyclopropyl formation is the rate-limiting step in both HO_2 and OH production from Cl-initiated oxidation at 296 K.

The sharp rise in the total yield of HO_2 at about 600 K is similar to that observed in other R + O_2 reactions. This sharp rise in HO_2 yield coincides with the emergence of double-exponential behavior in the HO_2 time profiles. At 296 K the rise time of the HO_2 signal is limited by the Cl + *c*-C_3H_6 reaction, but this reaction is not rate-limiting at higher temperature; Knox and Nelson[27] measured an activation energy of 4 kcal mol^{-1} for Cl + *c*-C_3H_6. As seen in Figure 1, the HO_2 formation rate constant increases as the temperature is increased between 296 and 683 K. At 623 and 683 K the HO_2 signal from *c*-C_3H_5 + O_2 displays a biexponential rise. This behavior is particularly apparent in the 683 K signal, where the fast initial rise in the HO_2 signal is not temporally resolved and a slower secondary rise appears with a pseudo-first-order rate constant of 1700 ± 220 s^{-1}. This component is much slower than the Cl + *c*-C_3H_6 reaction, and its existence indicates that a second HO_2 channel is occurring at these higher temperatures. The onset of this double-exponential formation of HO_2 corresponds with the sharp increase in the peak amplitude of the HO_2 signal with increasing temperature near 600 K.

3.2. Relative Rate Study of $k_{c\text{-}C_3H_5+O_2}/k_{c\text{-}C_3H_5+Cl_2}$ at Ford. In the presence of oxygen, there is a competition between Cl_2 and O_2 for the *c*-C_3H_5 radicals.

$$c\text{-}C_3H_5 + Cl_2 \rightarrow c\text{-}C_3H_5Cl + Cl \qquad (13)$$

$$c\text{-}C_3H_5 + O_2 \rightarrow \text{products} \qquad (14)$$

This competition was studied by subjecting *c*-$C_3H_6/Cl_2/O_2/N_2$ mixtures to UV irradiation and measuring the resulting *c*-C_3H_5Cl yield. Initial concentrations were 97−210 mTorr of *c*-C_3H_6, 1.0 Torr of Cl_2, and 0.047−10.1 Torr of O_2 in 700 Torr of N_2 at 296 K. Consistent with expectations, as the $[O_2]/[Cl_2]$ ratio was increased, the yield of *c*-C_3H_5Cl decreased. Figure 6 shows a plot of the reciprocal of the molar *c*-C_3H_5Cl yield versus $[O_2]/[Cl_2]$. If reactions 13 and 14 are the sole loss mechanisms for *c*-C_3H_5 radicals in the system, we expect that such a plot should be linear (with a slope = k_{14}/k_{13}) with a *y*-axis intercept of unity. As seen from Figure 6, these expectations are met. Linear least-squares analysis of the data in Figure 6 gives $k_{14}/k_{13} = 0.44 \pm 0.02$ in 700 Torr total pressure of N_2 at 296 K. Experiments in 75 and 10 Torr of N_2 diluent gave values of $k_{14}/k_{13} = 0.44 \pm 0.03$ and 0.24 ± 0.02. The decrease in k_{14}/k_{13} at 10 Torr presumably reflects the falloff behavior of the *c*-C_3H_5 + O_2 reaction. The magnitude of the falloff is consistent with expectations for an alkyl radical of the size of *c*-C_3H_5; for example, $k(C_2H_5 + O_2)$ also decreases by a factor of 2 over the pressure range 700−10 Torr.[41]

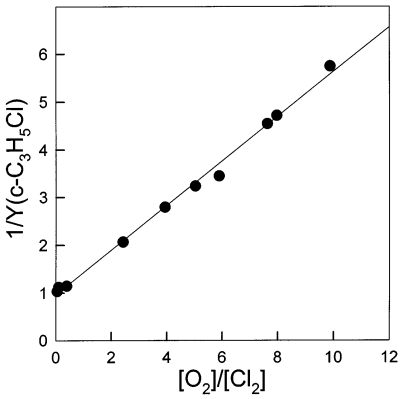

Figure 6. Plot of the reciprocal of the molar yield of *c*-C_3H_5Cl observed following the UV irradiation of *c*-$C_3H_6/Cl_2/O_2$ mixtures in 700 Torr of N_2 diluent at 296 K versus $[O_2]/[Cl_2]$.

3.3. Products following Reaction of *c*-C_3H_5 Radicals with O_2 Studied at Ford. To investigate the products formed following the reaction of *c*-C_3H_5 radicals with O_2, experiments were performed using *c*-C_3H_6/Cl_2 mixtures in 700 Torr of air. CO and CO_2 were the only products observed in such experiments. At 700 Torr total pressure, many of the possible primary products of the Cl atom-initiated oxidation of cyclopropane (e.g., acrolein, propene, ethene, allene) are 2 to 3 orders of magnitude more reactive toward Cl atoms than cyclopropane. For experiments employing consumptions of cyclopropane that were directly measurable (i.e., typically 10−50%), the loss of such primary products from secondary reaction with Cl will be severe.

To search for primary products, a series of experiments was performed at low total pressure (6−50 Torr) using mixtures of 500−550 mTorr of *c*-C_3H_6, 10 mTorr of C_2H_5Cl, 25−50 mTorr of Cl_2, and 5 Torr of O_2 made up to 6−50 Torr total pressure with N_2 diluent. To operate under conditions where secondary reactions involving Cl atoms are modest, we need to conduct experiments in which the consumption of cyclopropane is small (i.e., 1−2%). Such consumptions are difficult to measure directly but can be measured with sufficient precision indirectly using a "tracer" method. C_2H_5Cl serves as a convenient tracer. Cl atoms react 70 times more rapidly with C_2H_5Cl than with cyclopropane. By monitoring the loss of C_2H_5Cl, the consumption of cyclopropane can be calculated. Using this approach, C_2H_4 (ethene) and C_2H_4O (oxirane) were identified as products. Figure 7 shows IR spectra obtained before (A) and after (B) irradiation of a mixture of 500−550 mTorr of *c*-C_3H_6, 10 mTorr of C_2H_5Cl, 25−50 mTorr of Cl_2, and 5 Torr of O_2. Subtraction of panel A from B gives panel C, which, when compared with reference spectra of C_2H_4 (D) and C_2H_4O (E), shows the formation of these species. Figure 8 shows a plot of the formation of C_2H_4 (bottom panel) and C_2H_4O (top panel) versus cyclopropane loss for experiments conducted in 6 Torr total pressure at 296 K. Open symbols are the observed data; filled symbols have been corrected for secondary loss by reaction with Cl atoms. Corrections were computed using the value of k_4 measured in the accompanying work and published kinetic data for $k(Cl + C_2H_4)$[42] and $k(Cl + C_2H_4O)$.[43] Linear least-squares analysis of the corrected data gives molar yields for C_2H_4 and C_2H_4O of 0.11 ± 0.03 and 0.14 ± 0.02. Experiments in 10 and 50 Torr total pressure give molar yields for C_2H_4O of 0.08 ± 0.02 (10 Torr) and 0.06 ± 0.02 (50 Torr) and for C_2H_4 of 0.15 ± 0.01 (10 Torr) and 0.30 ± 0.06 (50 Torr).

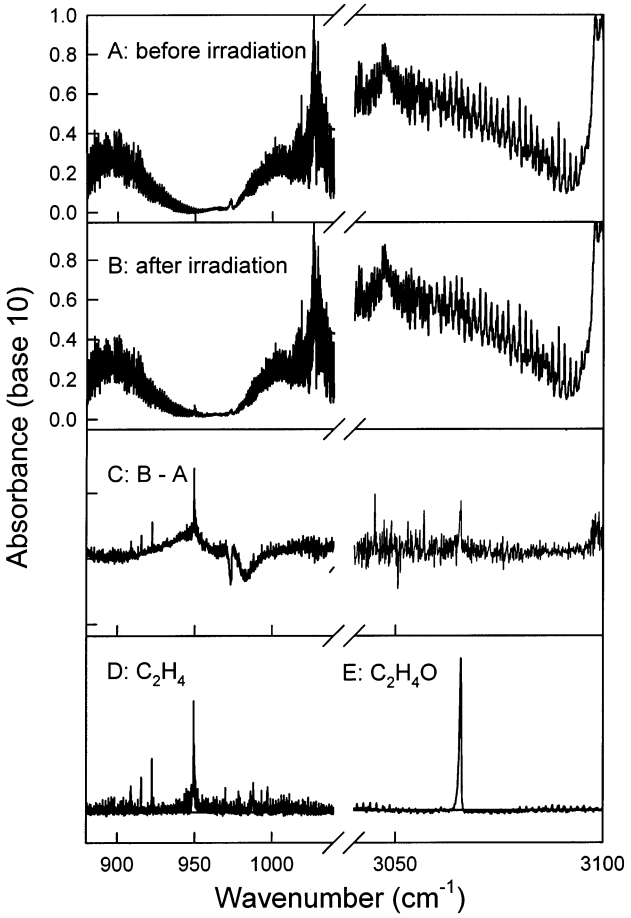

Figure 7. IR spectra acquired before (A) and after (B) a 3 min irradiation of a mixture of 496 mTorr of *c*-C_3H_6, 11 mTorr of C_2H_5Cl, and 49 mTorr of Cl_2 in 6 Torr total pressure of O_2 diluent. Subtraction of A from B gives C (the negative feature at approximately 970 cm^{-1} reflects the consumption of C_2H_5Cl during the experiment). Reference spectra of C_2H_4 and C_2H_4O are given in panels D and E.

3.4. Computational Study of Cyclopropyl + O_2 Reaction. The calculated energies for various stationary points on the cyclopropyl + O_2 potential energy surface are listed in Tables 5 and 6 and depicted schematically in Figure 9. The well depth of the cyclopropylperoxy radical (II) is calculated to be 42.1 kcal mol^{-1} relative to the cyclopropyl + O_2 reactants (I). This well is significantly deeper than that for other alkyl + O_2 additions. The direct elimination of HO_2, which is a dominant channel in ethyl, propyl, and butyl + O_2 reactions, must overcome a sizable barrier (3.9 kcal mol^{-1} relative to reactants) in cyclopropyl + O_2, since the overall reaction to form cyclopropene + HO_2 (VIII) is endothermic. However, because of the energy available in the cyclopropyl radical, a number of isomerization pathways are accessible. The lowest-energy transition state for isomerization of the cyclopropylperoxy radical is calculated to be the internal 1,5s isomerization to form the hydroperoxycyclopropyl species IV. This radical may subsequently ring-open to form a $CH_2CHCHOOH$ radical (IX) or rearrange and dissociate to form OH + acrolein (X). The implication of the quantum chemistry is that OH + acrolein should be the principal bimolecular products.

A second isomerization pathway is possible: a breaking of the cyclopropyl ring in conjunction with the formation of a C−O−O dioxirane ring species (III). The transition state for this isomerization is calculated to be 0.5 kcal mol^{-1} above the reactants. (It is worth noting that the large spin contamination for this transition state suggests a large uncertainty in this energy (e.g. at least 3−4 kcal mol^{-1}) and for many of the other transition state energies, which also have significant spin contaminations.) The dioxirane species III has several conceivable rearrangement pathways, some of which may be plausible

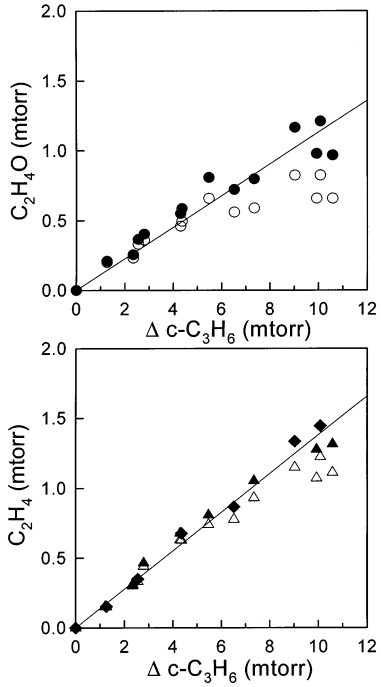

Figure 8. Plot of the formation of C_2H_4 (bottom panel) and C_2H_4O (top panel) versus the loss of *c*-C_3H_6 following UV irradiation of a mixture of 496−544 mTorr of *c*-C_3H_6, 11 mTorr of C_2H_5Cl, and 49−103 mTorr of Cl_2 in 5 Torr total pressure of O_2 diluent at 296 K. Filled symbols are observed data; open symbols show the effect of correcting for secondary reactions with Cl atoms. See text for details.

TABLE 5: Calculated Energies of Stable Species on the Cyclopropyl + O_2 System[a]

stationary point	energy (kcal mol^{-1}) relative to *c*-C_3H_5 + O_2
I. *c*-C_3H_5 + O_2	0.0
II. *c*-C_3H_5•O_2	−42.1
III. •$CH_2CH_2C(H)OO$ (C−O−O ring)	−39.4
IV. *c*-C_3H_4OOH	−20.1
V. allyl + O_2	−28.4
VI. allyl•O_2	−48.5
VII. •$OCH_2CH_2C(O)H$	−97.6
VIII. *c*-C_3H_4 + HO_2	0.6
IX. $CH_2CHCHOOH$	−50.6
X. $CH_2CHC(O)H$ + OH	−77.5
XI. CH_2CCH_2 + HO_2	−21.7

[a] Calculated at the HL1 level.

TABLE 6: Calculated Transition State Energies in the Cyclopropyl + O_2 System

	energy[a] (kcal mol^{-1})		$\langle S^2 \rangle$	
stationary point	HL1	HL2	B3LYP	HF
TS I → V	23.3		0.81	1.17
TS II → III	3.8	0.5	0.78	1.01
TS II → IV	−4.7	−3.6	0.76	0.79
TS II → VI	4.2	5.8	0.75	0.78
TS II → VII	6.5	1.4	0.77	1.51
TS II → VIII	3.9		0.76	0.81
TS IV → IX	−1.8		0.77	1.15
TS IV → X	0.6		0.80	1.19
TS VI → X	−8.7		0.77	1.16
TS VI → XI	−9.0		0.76	0.82

[a] Relative to *c*-C_3H_5 + O_2.

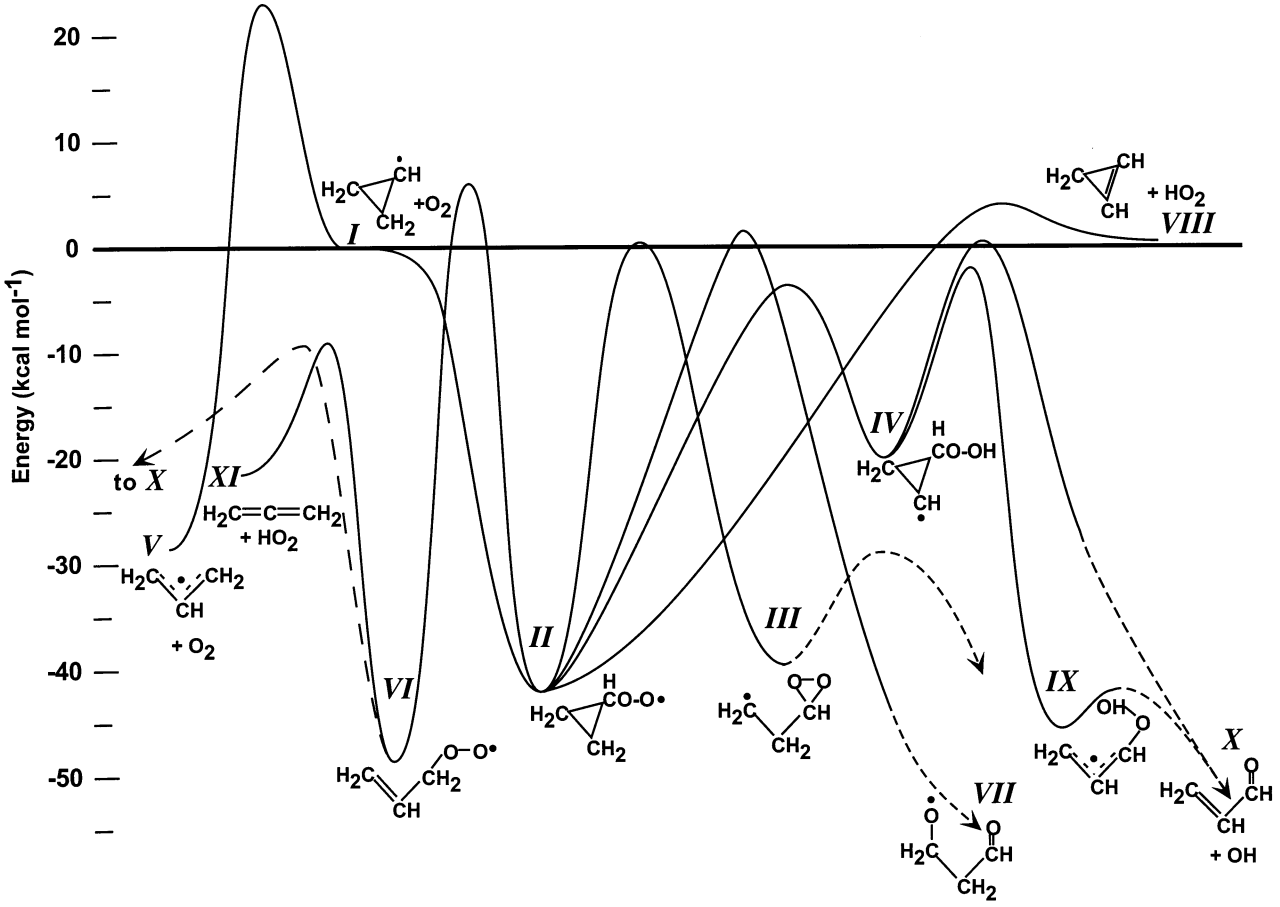

Figure 9. Schematic potential energy surface for the cyclopropyl + O_2 reaction, showing stationary point energies calculated at the HL1 level, except transition states II → III, II → IV, II → VI, and II → VII at the HL2 level.

intermediates to ethene + HCO_2 or oxirane + HCO. Also, formation of formaldehyde + vinoxy (CH_2CHO) is the most likely consequence of isomerization to the $CH_2(O)CH_2CHO$ species (VII), which proceeds via a transition state calculated at 1.4 kcal mol^{-1} above cyclopropyl + O_2. Finally, formation of the allylperoxy radical (VI) is calculated to proceed over a moderately high (5.8 kcal mol^{-1}) barrier; however, this pathway to allyl + O_2 is much more favorable than direct ring-opening of cyclopropyl, which must traverse a 23.3 kcal mol^{-1} barrier.

4. Discussion

The present measurements of HO_2 and OH production in the Cl-initiated oxidation of cyclopropane can be compared to similar observations in other alkane oxidations. The formation of significant OH is unusual for an alkyl + O_2 reaction, but the quantum chemical calculations clearly predict this behavior. The primary products from cyclopropyl + O_2 are predicted to be CH_2CHCHO + OH (X in Figure 9), arising from an H transfer from the ring to the terminal O atom (IV in Figure 9), followed by cyclopropyl ring-opening and O−O bond fission. The maximum barrier for this process is 1.8 kcal mol^{-1} below reactants, and so the overall reaction should be fairly rapid.

While the observation of significant OH production even at room temperature is peculiar to the cyclopropyl + O_2 system, the HO_2 production is ostensibly similar to that of other alkyl + O_2 reactions. The contributions of "prompt" and "delayed" components of HO_2 observed at the higher temperatures of the present work are common to the previously reported investigations of time-resolved HO_2 production in alkyl + O_2 reactions. The sharp rise in the peak amplitudes of the HO_2 signal at ~600 K from *c*-C_3H_5 + O_2 appears at about the same temperature as that for a similar sharp rise in the total HO_2 yield in other alkyl reactions studied.[1,2,5,6,8,12,13] This similarity encourages discussion of the cyclopropyl + O_2 reaction within the framework established for other R + O_2 systems. The HO_2 production for many R + O_2 reactions has been modeled by a coupled reaction scheme,[2,3,7,18,21]

$$\mathrm{R} + \mathrm{O_2} \xrightarrow{k_a} \text{alkene} + \mathrm{HO_2}$$

$$\mathrm{R} + \mathrm{O_2} \underset{}{\overset{k_b[\mathrm{M}]}{\longleftrightarrow}} \mathrm{RO_2} \xrightarrow{k_e[\mathrm{M}]} \text{alkene} + \mathrm{HO_2}\,, \qquad \mathrm{RO_2} \xrightarrow{} \textit{removal}$$

where k_e represents thermal elimination of HO_2 from RO_2 and k_a represents direct production of HO_2 and alkene from the reactants, that is, elimination of the HO_2 from the excited alkylperoxy adduct prior to stabilization.[3,7,18] The kinetics of eq 15 give a biexponential production of HO_2 products, where the rates of formation and amplitudes depend on all the rate coefficients of the system. The reaction of cyclopropyl radical with O_2 must include a similar reversible addition to form cyclopropylperoxy. However, a number of exothermic ring-opening product channels are available to *c*-$C_3H_5O_2$. Further, formation of cyclopropene + HO_2 is endothermic, making any significant contribution of the elimination channel extremely unlikely. It therefore seems probable that, despite its superficial similarity to other alkyl + O_2 reactions, a different mechanism is responsible for HO_2 production in the cyclopropane oxidation.

In addition to providing a pathway for HO_2 formation, the mechanism must also be consistent with the increase in formation of HO_2 at higher temperatures. If a mechanism is found for HO_2 production from cyclopropyl + O_2 that competes with formation of stabilized *c*-$C_3H_5O_2$, this second demand is relatively easily met. The onset of thermal dissociation of the cyclopropylperoxy radical at elevated temperatures will naturally provide both a biexponential appearance of the products of the *c*-C_3H_5 + O_2 reaction and an increase in the importance of bimolecular channels.

There are several conceivable primary and secondary reaction channels that could provide an explanation for HO_2 production in the *c*-C_3H_5 + O_2 reaction. Several possibilities can be eliminated as inconsistent with the experimental or quantum chemical evidence. First is an alternative elimination pathway for HO_2 formation. Production of allene + HO_2 (XI in Figure 9) is exothermic from cyclopropyl + O_2, but this elimination from *c*-$C_3H_5O_2$ must proceed through a constrained four-membered-ring transition state. A transition state for such an isomerization is calculated to lie at 7.3 kcal mol^{-1} at the HL1 level, energetically inaccessible under the present conditions. Further, the isomerization leads not to allene + HO_2 but to OH + cyclopropanone.

Another conceivable source of HO_2 is through isomerization of the cyclopropyl radical to the allyl radical. The cyclopropyl radical isomerization rate constant has been reported as $2.51 \times 10^{10} \exp(-9611K/T)$ s^{-1},[44] which corresponds to a first-order rate constant of 27 000 s^{-1} at 700 K. However, the reaction of the allyl radical with O_2 does not produce significant HO_2 under the conditions of these experiments.[45,46] Observation of HO_2 formation from the reaction of allyl + O_2 was attempted between 296 and 668 K, employing the reaction of Cl + CH_3CHCH_2 to form the allyl radical. No measurable HO_2 was observed from this reaction, and it is concluded that the reaction of allyl + O_2 cannot be responsible for the observed HO_2 production in cyclopropane oxidation. In fact, the slight decrease in the HO_2 yield as the temperature is increased from 673 to 700 K may be due to the increased loss of cyclopropyl radicals to form the allyl radical.

Finally, production of HO_2 from secondary reactions of the cyclopropylperoxy radicals must be considered. The self-reaction of *c*-$C_3H_5O_2$ radicals may produce cyclopropoxy radicals, which could react, for example, with O_2 to form HO_2 + cyclopropanone. The cyclopropylperoxy self-reaction has not been measured. However, the self-reactions of analogous RO_2 radicals are far too slow to account for the observed time scale of HO_2 production. For example, the self-reaction of *n*-C_3H_7OO radicals has a rate coefficient at 298 K of $\sim 3 \times 10^{-13}$ cm^3 molecule^{-1} s^{-1},[28] which would give a half-life of $\sim$0.1 s at the radical densities of the current experiments. The cyclopropylperoxy self-reaction would have to be $\sim$100 times faster than other alkylperoxy radical self-reactions to be responsible for the observed HO_2 production. However, the hydroperoxy alkyl radical (IV) isomer of *c*-$C_3H_5O_2$ may react with O_2. Reactions of similar species are important for chain branching in hydrocarbon oxidation,[47] and the subsequent chemistry may be responsible for some of the observed HO_2.

A final possibility is that HO_2 formation in the cyclopropyl + O_2 reaction proceeds via further reaction of HCO or HOCO products. The barrier to formation of a COO ring in concert with cyclopropyl ring-opening (II → III) is 0.5 kcal mol^{-1} above the reactants at the present level of calculations, and the transient species formed by this isomerization would be energized and may yield secondary products. In particular, the OO fission of the CO_2 ring, with a barrier significantly below reactants, could yield a variety of products, such as H_2CO + CH_2CHO, C_2H_4 + HCO_2, and/or C_2H_4O + HCO. Either HCO or HCO_2 products could rapidly yield HO_2 by reaction with O_2, thereby explaining the observed prompt formation of HO_2. The observation in the present smog chamber experiments of both oxirane and ethene as products in the oxidation of cyclopropane is consistent with a significant role for this pathway. Alternatively, an O transfer in conjunction with cyclopropyl ring-opening from the initial adduct (II → VII) is predicted to lie 1.4 kcal mol^{-1} above reactants. The resulting OCH_2CH_2CHO species might again yield HCO + C_2H_4O. At the present level of theory, the quantum chemical calculations predict that the transition states for these pathways are at higher energy than reactants, in disagreement with the implications of the experiments. However, the estimated uncertainties in these calculations (3−4 kcal mol^{-1}) exceed the calculated endothermicities. The quantum chemistry therefore suggests isomerization to III or VII as the most plausible precursors to oxirane or ethene production.

The formation of OH further complicates modeling the *c*-C_3H_5 + O_2 system, since reactions of OH can form additional HO_2 by secondary chemistry. The OH radical can react with cyclopropane to form another cyclopropyl radical, which will react with O_2 to create more OH and HO_2. This chain reaction will tend to convert OH into the less reactive HO_2 or cyclopropylperoxy radicals. The *c*-C_3H_6 + OH reaction has a significant activation energy ($k = (6.01 \times 10^{-13}$ cm^3 molecule^{-1} s^{-1})$(T/298\text{ K})^{1.5}e^{(-521K/T)}$).[48−50] An increased role of this reaction may also contribute to the increase in HO_2 as the temperature is increased. Reactions of RO_2 radicals with OH could also conceivably produce HO_2, although there appears to be little experimental investigation of such reactions. This reaction could be relatively fast; it is an exothermic radical−radical reaction, and the similar reaction of $C_2H_5O_2$ + OH is calculated to proceed without a barrier.[51] Biggs and co-workers[52] report $k = 4 \times 10^{-11}$ cm^3 molecule^{-1} s^{-1} for CF_3O_2 + OH → HO_2 + CF_3O at 296 K. The possibility of contributions from a similar reaction, *c*-$C_3H_5O_2$ + OH → HO_2 + *c*-C_3H_5O (cyclopropoxy), cannot be excluded in the present system, and if this reaction occurs, it may compete with HO_2 formation by the pathways described above. However, the rapid rise of the HO_2 concentration is not consistent with exclusive production from the RO_2 + OH reaction, which would produce a sigmoidal rise. Direct investigations of the kinetics and branching fractions of RO_2 + OH reactions would be helpful in determining whether these reactions may be important in modeling low-temperature oxidation of hydrocarbons. Recent measurements of correlated photofragment and photoelectron energies in dissociative photodetachment of the cyclopropoxide ion imply that dissociation of the cyclopropoxy radical to form HCO + C_2H_4 is exothermic by (6.2 ± 1.6) kcal mol^{-1}.[53] In the same work the barrier to dissociation is calculated (at the QCISD(T)/6-311+G* level) to be only $\sim$12 kcal mol^{-1}. The present HL2 calculations yield a reaction enthalpy for cyclopropoxy dissociation of $\Delta H_{298}^\circ = +4.8$ kcal mol^{-1}. Nonetheless, the cyclopropoxy radical, formed either by OH + RO_2 or RO_2 + RO_2, could provide a pathway for ethene formation via reaction of the stabilized RO_2 species, consistent with the present observation of an increase of the overall C_2H_4 yield at 298 K with increasing total pressure.

The proposed empirical *c*-C_3H_5 + O_2 reaction mechanism predicts the formation of ethene or oxirane, as observed in the smog chamber measurements, will coincide with production of HO_2 via secondary reaction of the HCO_2 or HCO coproduct with O_2. This identification would predict a total HO_2 yield at

TABLE 7: Reactions and Rate Constants Used in the Qualitative Model for the Time-Resolved HO_2 and OH Signals from Cl-Initiated Oxidation at 298 K

reaction	$k_{298\ K}$ (cm^3 $molecule^{-1}$ s^{-1})	ref
$c\text{-}C_3H_6 + Cl \rightarrow HCl + c\text{-}C_3H_5$	1.15×10^{-13}	26
$c\text{-}C_3H_6 + OH \rightarrow H_2O + c\text{-}C_3H_5$	7.6×10^{-14}	48, 49
$c\text{-}C_3H_5 + Cl_2 \rightarrow Cl + c\text{-}C_3H_5Cl$	2×10^{-11}	*a*
$c\text{-}C_3H_5 + O_2 \rightarrow HCO + C_2H_4O$	3.8×10^{-13}	this work
$c\text{-}C_3H_5 + O_2 \rightarrow HCO_2 + C_2H_4$	7.2×10^{-13}	this work
$c\text{-}C_3H_5 + O_2 \rightarrow c\text{-}C_3H_5O_2$	3.0×10^{-12}	this work
$c\text{-}C_3H_5 + O_2 \rightarrow OH + C_3H_4O$	5.8×10^{-13}	this work
$OH + HO_2 \rightarrow H_2O + O_2$	1.1×10^{-10}	30
$HO_2 + HO_2 \rightarrow H_2O_2 + O_2$	1.66×10^{-12}	30
$HCO + O_2 \rightarrow HO_2 + CO$	5.6×10^{-12}	59
$HCO_2 + O_2 \rightarrow HO_2 + CO_2$	2.1×10^{-12}	*b*
$Cl + HO_2 \rightarrow OH + ClO$	9.4×10^{-12}	30
$Cl + HO_2 \rightarrow HCl + O_2$	3.5×10^{-11}	30
$OH + c\text{-}C_3H_5O_2 \rightarrow HO_2 + c\text{-}C_3H_5O$	4×10^{-11}	*c*
$HO_2 + c\text{-}C_3H_5O_2 \rightarrow$ products	8×10^{-12}	*d*
$c\text{-}C_3H_5O_2 + c\text{-}C_3H_5O_2 \rightarrow$ products	1×10^{-13}	*e*

[a] Estimated from $C_2H_3 + Cl_2$, ref 61. [b] Estimated from $HOCO + O_2$, ref 62. [c] Estimated on the basis of $OH + CF_3O_2$, ref 52. [d] Estimated on the basis of other $HO_2 + RO_2$ reactions, ref 63. [e] Estimated on the basis of other RO_2 self-reactions, ref 63.

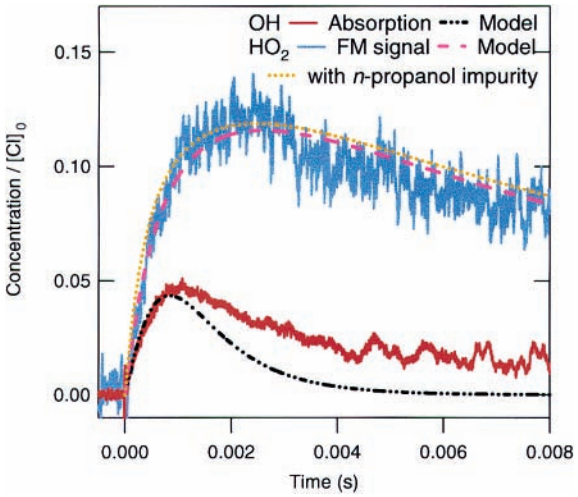

Figure 10. Predicted HO_2 and OH signals at 296 K from the qualitative model of Cl-initiated oxidation compared to the signals from Figure 3. The branching fraction of $c\text{-}C_3H_5 + O_2 \rightarrow OH + C_3H_4O$ is set at 0.12 to match the amplitude of the OH absorption signal, and the total branching fraction to ethene + HCO_2 and oxirane + HCO is set to 0.23 n the basis of the 10 Torr smog chamber measurements. The initial Cl atom density is estimated as 3×10^{13} cm^{-3}.

298 K of ~0.25 in the present experiments. To determine whether this value is consistent with the time-resolved FM measurements, a simplified kinetic model has been constructed on the basis of the proposed mechanism, assuming all ethene and oxirane is correlated with HO_2 production. This model predicts a peak $[HO_2]/[Cl]_0$ at 298 K of between ~0.1 and 0.2, depending on the values assumed for several unknown rate constants. The model assumes that the reaction of OH with $c\text{-}C_3H_5O_2$ proceeds to form HO_2 + cyclopropoxy radical with a rate constant of 4×10^{-11} cm^3 $molecule^{-1}$ s^{-1}, but it does not assume any subsequent reaction of the cyclopropoxy radical. (However, a model assuming rapid dissociation of the cyclopropoxy radical to HCO + ethene yields similar time traces for the same overall ethene yield, with slightly slower HO_2 production, if a 50% smaller direct HCO_2 + ethene branching fraction is used.) The details of the simplified mechanism are shown in Table 7, and predicted time-resolved OH and HO_2 signals are shown in Figure 10 compared with the data from Figure 3. The agreement is relatively good, suggesting that the data are consistent with HO_2 formation via secondary reactions of HCO and HCO_2. However, many rate constants and concentrations are unknown or estimated, and the model should be regarded as merely qualitative.

Possible contributions of reactions of *n*-propanol impurities to the HO_2 signal must also be addressed. The difference between rate coefficients derived from time-resolved measurements of HCl formation and those derived from relative rate measurements of cyclopropane disappearance is ~20%.[26] This discrepancy is consistent with ~0.08% impurity, with the composition measured by GC. The calculated change in the HO_2 concentration for this level of *n*-propanol impurity is minimal, as shown by the dotted orange line in Figure 10. Even if the 20% difference in apparent rate constants between the two methods were entirely due to reaction with *n*-propanol, the measured HO_2 signal at 296 K (where the effect should be greatest) would be changed by approximately 15%. As the temperature is increased, the predicted maximum contribution of *n*-propanol impurities to the HO_2 signal rapidly becomes negligible.

Detailed comparison of the end product analysis from the FTIR smog chamber studies and the time-resolved infrared absorption measurements of product formation requires consideration of the differing time scales of the two experiments. The time-resolved infrared absorption experiments are most sensitive to rapidly formed products, while the smog chamber experiments have longer residence times. The peak $[HO_2]/[Cl]_0$ at 296 K in the FM measurements decreases slightly with increasing pressure between 10 and 75 Torr, and the sum of the oxirane and ethene yields in the smog chamber experiments is roughly constant between 6 and 50 Torr (0.25 ± 0.05 at 6 Torr, 0.23 ± 0.03 at 10 Torr, 0.36 ± 0.8 at 50 Torr). However, if ethene is also an end product of $c\text{-}C_3H_5O_2$ reactions, it is possible that any HO_2 formed in conjunction with that process would appear on too long a time scale to be evident in the time-resolved experiments. In particular, the reactions of the cyclopropoxy radical, neglected in the simple qualitative mechanism, may be a source of ethene (and HO_2) on a longer time scale.

5. Conclusions

In summation, the experimental evidence is consistent with a proposed mechanism for the cyclopropyl + O_2 reaction that proceeds via ring-opening to HCO + oxirane, OH + acrolein, and HCO_2 + ethene products. The formation of these bimolecular products competes with stabilization of the cyclopropylperoxy adduct and formation of the $c\text{-}C_3H_4OOH$ isomer. Future work may be needed to clarify the role of the hydroperoxyalkyl isomer in the overall oxidation system. The rise with temperature of both HO_2 and OH yields above ~600 K is attributed to the onset of thermal $c\text{-}C_3H_5O_2$ dissociation. The branching fractions deduced from comparing a simple qualitative kinetic model to the present experimental data at 296 K suggest ~10−15% branching into OH + other products and a total of ~25% branching into (HCO + oxirane) and (HCO_2 + ethene). However, such branching fractions remain inconsistent with the quantum chemical calculations, which suggest that stabilization to cyclopropylperoxy should dominate the reaction and that OH + acrolein should be the most significant bimolecular products.

Acknowledgment. We thank Dr. John Farrell (ExxonMobil Corporation) for help in conducting the experiments at Ford. The work at Sandia National Laboratories (J.D.D., C.A.T.,

S.J.K.) is supported by the Division of Chemical Sciences, Geosciences, and Biosciences, the Office of Basic Energy Sciences, the U. S. Department of Energy. Sandia is a multiprogram laboratory operated by Sandia Corporation, a Lockheed Martin Company, for the United States Department of Energy under Contract DE-AC04-94-AL85000.

References and Notes

(1) DeSain, J. D.; Clifford, E. P.; Taatjes, C. A. *J. Phys. Chem. A* **2001**, *105*, 3205.
(2) Clifford, E. P.; Farrell, J. T.; DeSain, J. D.; Taatjes, C. A. *J. Phys. Chem. A* **2000**, *104*, 11549.
(3) Miller, J. A.; Klippenstein, S. J.; Robertson, S. H. *Proc. Combust. Inst.* **2000**, *28*, 1479.
(4) Kaiser, E. W.; Wallington, T. J. *J. Phys. Chem.* **1996**, *100*, 18770.
(5) Kaiser, E. W. *J. Phys. Chem.* **1995**, *99*, 707.
(6) Kaiser, E. W. *J. Phys. Chem. A* **1998**, *102*, 5903.
(7) Rienstra-Kiracofe, J. C.; Allen, W. D.; Schaefer, H. F., III. *J. Phys. Chem A* **2000**, *104*, 9823.
(8) Kaiser, E. W. *J. Phys. Chem. A* **2002**, *106*, 1256.
(9) Baker, R. R.; Baldwin, R. R.; Walker, R. W. *Trans. Faraday Soc.* **1970**, *66*, 3016.
(10) Baldwin, R. R.; Cleugh, C. J.; Walker, R. W. *J. Chem. Soc., Faraday Trans. 1* **1976**, *72*, 1715.
(11) Baldwin, R. R.; Pickering, I. A.; Walker, R. W. *J. Chem. Soc., Faraday Trans. 1* **1980**, *76*, 2374.
(12) DeSain, J. D.; Taatjes, C. A. *J. Phys. Chem. A* **2001**, *105*, 6646.
(13) DeSain, J. D.; Taatjes, C. A.; Miller, J. A.; Klippenstein, S. J.; Hahn, D. K. *Faraday Discuss.* **2001**, *119*, 101.
(14) Gulati, S. K.; Walker, R. W. *J. Chem. Soc., Faraday Trans. 2* **1988**, *84*, 401.
(15) Handford-Styring, S. M.; Walker, R. W. *J. Chem. Soc., Faraday Trans* **1995**, *91*, 1431.
(16) Handford-Styring, S. M.; Walker, R. W. *Phys. Chem. Chem. Phys.* **2002**, *4*, 620.
(17) Kaiser, E. W.; Lorkovic, I. M.; Wallington, T. J. *J. Phys. Chem.* **1990**, *94*, 3352.
(18) Miller, J. A.; Klippenstein, S. J. *Int. J. Chem. Kinet.* **2001**, *33*, 654.
(19) Slagle, I. R.; Feng, Q.; Gutman, D. *J. Phys. Chem.* **1984**, *88*, 3648.
(20) Slagle, I. R.; Park, J.-Y.; Gutman, D. *Proc. Combust. Inst.* **1984**, *20*, 733.
(21) Wagner, A. F.; Slagle, I. R.; Sarzynski, D.; Gutman, D. *J. Phys. Chem.* **1990**, *94*, 1853.
(22) Walker, R. W.; Morley, C. Basic Chemistry of Combustion. In *Low-Temperature Combustion and Autoignition*; Pilling, M. J., Ed.; Elsevier: Amsterdam, 1997; p 1.
(23) Simon, V.; Simon, Y.; Scacchi, G.; Baronnet, F. *Can. J. Chem.* **1997**, *75*, 575.
(24) Handford-Styring, S. M.; Walker, R. W. *Phys. Chem. Chem. Phys.* **2001**, *3*, 2043.
(25) Falconer, W. E.; Knox, J. H.; Trotman-Dickinson, A. F. *J. Chem. Soc.* **1961**, 782.
(26) Hurley, M. D.; Schneider, W. F.; Wallington, T. J.; DeSain, J. D.; Taatjes, C. A. *J. Phys. Chem. A* **2003**, *107*, 2003.
(27) Knox, J. H.; Nelson, R. L. *Trans. Faraday Soc.* **1959**, *55*, 937.
(28) Atkinson, R.; Baulch, D. L.; Cox, R. A.; Hampson, R. F., Jr.; Kerr, J. A.; Rossi, M. J.; Troe, J. *J. Phys. Chem. Ref. Data* **1997**, *26*, 521.
(29) Cheema, S. A.; Holbrook, K. A.; Oldershaw, G. A.; Walker, R. W. *Int. J. Chem. Kinet.* **2001**, *34*, 110.
(30) DeMore, W. B.; Sander, S. P.; Golden, D. M.; Hampson, R. F.; Kurylo, M. J.; Howard, C. J.; Ravishankara, A. R.; Kolb, C. E.; Molina, M. J. *Chemical Kinetics and Photochemical Data for Use in Stratospheric Modeling*; Jet Propulsion Laboratory: Pasadena, CA, 1997.
(31) Tyndall, G. S.; Wallington, T. J.; Hurley, M. D.; Schneider, W. F. *J. Phys. Chem.* **1993**, *97*, 1576.
(32) Wallington, T. J.; Japar, S. M. *J. Atmos. Chem.* **1989**, 399.
(33) Becke, A. D. *J. Chem. Phys.* **1993**, *98*, 5648.
(34) Hehre, W. J.; Radom, L.; Pople, J. A.; Schleyer, P. v. R. *Ab Initio Molecular Orbital Theory*; Wiley: New York, 1987.
(35) Curtiss, L. A.; Raghavachari, K.; Redfern, P. C.; Rassolov, V.; Pople, J. A. *J. Chem. Phys.* **1998**, *109*, 7764.
(36) Martin, J. M. L. *Chem. Phys. Lett.* **1996**, *269*, 669.
(37) Dunning, T. H. *J. Chem. Phys.* **1989**, *90*.
(38) Frisch, M. J.; Trucks, G. W.; Schlegel, H. B.; Scuseria, G. E.; Robb, M. A.; Cheeseman, J. R.; Zakrzewski, V. G.; Montgomery, J. A., Jr.; Stratmann, R. E.; Burant, J. C.; Dapprich, S.; Millam, J. M.; Daniels, A. D.; Kudin, K. N.; Strain, M. C.; Farkas, O.; Tomasi, J.; Barone, V.; Cossi, M.; Cammi, R.; Mennucci, B.; Pomelli, C.; Adamo, C.; Clifford, S.; Ochterski, J.; Petersson, G. A.; Ayala, P. Y.; Cui, Q.; Morokuma, K.; Malick, D. K.; Rabuck, A. D.; Raghavachari, K.; Foresman, J. B.; Cioslowski, J.; Ortiz, J. V.; Stefanov, B. B.; Liu, G.; Liashenko, A.; Piskorz, P.; Komaromi, I.; Gomperts, R.; Martin, R. L.; Fox, D. J.; Keith, T.; Al-Laham, M. A.; Peng, C. Y.; Nanayakkara, A.; Gonzalez, C.; Challacombe, M.; Gill, P. M. W.; Johnson, B.; Chen, W.; Wong, M. W.; Andres, J. L.; Gonzalez, C.; Head-Gordon, M.; Replogle, E. S.; Pople, J. A. *GAUSSIAN 98*; Gaussian, Inc.: Pittsburgh, PA, 1998.
(39) Pilgrim, J. S.; McIlroy, A.; Taatjes, C. A. *J. Phys. Chem. A* **1997**, *101*, 1873.
(40) Baghal-Vayjooee, M. H.; Benson, S. W. *J. Am. Chem. Soc.* **1979**, *101*, 2838.
(41) Kaiser, E. W.; Wallington, T. J.; Andino, J. M. *Chem. Phys. Lett.* **1990**, *168*, 309.
(42) Kaiser, E. W.; Wallington, T. J. *J. Phys. Chem.* **1996**, *100*, 4111.
(43) Ponomarev, D.; Hurley, M. D.; Wallington, T. J. *Int. J. Chem. Kinet.* **2002**, *34*, 122.
(44) Kerr, J. A.; Smith, A.; Trotman-Dickinson, A. F. *J. Chem. Soc. A* **1969**, *9*, 399.
(45) Lodhi, Z. H.; Walker, R. W. *J. Chem. Soc., Faraday Trans.* **1991**, *87*, 681.
(46) Stothard, N. D.; Walker, R. W. *J. Chem. Soc., Faraday Trans.* **1992**, *88*, 2621.
(47) Curran, H. J.; Gaffuri, P.; Pitz, W. J.; Westbrook, C. K. *Combust. Flame* **1998**, *114*, 149.
(48) DeMore, W. B.; Bayes, K. D. *J. Phys. Chem. A* **1999**, *103*, 2649.
(49) Clarke, J. S.; Kroll, J. H.; Donahue, N. M.; Anderson, J. G. *J. Phys. Chem. A* **1998**, *102*, 9847.
(50) Dobe, S.; Turanyi, T.; Iogansen, A. A.; Berces, T. *Int. J. Chem. Kinet.* **1992**, *24*, 191.
(51) DeSain, J. D.; Klippenstein, S. J.; Miller, J. A.; Taatjes, C. A. *J. Phys. Chem. A*, submitted.
(52) Biggs, P.; Canosa-Mas, C. E.; Shallcross, D. E.; Vipond, A.; Wayne, R. P. *J. Chem. Soc., Faraday Trans.* **1997**, *93*, 2701.
(53) Alconcel, L. S.; Deyerl, H.-J.; DeClue, M.; Continetti, R. E. *J. Am. Chem. Soc.* **2001**, *123*, 3125.
(54) Grotheer, H.; Riekert, G.; Walter, D.; Just, T. *J. Phys. Chem.* **1988**, *92*, 4028.
(55) Hess, W. P.; Tully, F. P. *J. Phys. Chem.* **1989**, *93*, 1944.
(56) Morley, C.; Smith, I. W. M. *J. Chem. Soc., Faraday Trans. 2* **1972**, *68*, 1016.
(57) Baulch, D. L.; Cobos, C. J.; Cox, R. A.; Esser, C.; Frank, P.; Just, T.; Kerr, J. A.; Pilling, M. J.; Troe, J.; Walker, R. W.; Warnatz, J. *J. Phys. Chem. Ref. Data* **1992**, *21*, 411.
(58) Tsang, W.; Herron, J. T. *J. Chem. Phys. Ref. Data* **1991**, *20*, 609.
(59) DeSain, J. D.; Jusinski, L. E.; Ho, A. D.; Taatjes, C. A. *Chem. Phys. Lett.* **2001**, *347*, 79.
(60) Pagsberg, P.; Munk, J.; Anastasi, C.; Simpson, V. J. *J. Phys. Chem.* **1989**, *93*, 5162.
(61) Timonen, R. S.; Russell, J. J.; Sarzynski, D.; Gutman, D. *J. Phys. Chem.* **1987**, *93*, 1873.
(62) Petty, J. T.; Harrison, J. A.; Moore, C. B. *J. Phys. Chem.* **1993**, *97*, 11194.
(63) Wallington, T. J.; Dagaut, P.; Kurylo, M. J. *Chem. Rev.* **1992**, *92*, 667.